

Coexchangeable process modelling for uncertainty quantification in joint climate reconstruction

Lachlan Astfalck¹, Daniel Williamson^{2,3}, Niall Gandy¹, Lauren Gregoire¹,
and Ruza Ivanovic¹

¹*School of Earth and Environment, The University of Leeds, Leeds, UK*

²*Department of Mathematical Sciences, Exeter University, Exeter, UK*

³*The Alan Turing Institute, British Library, London, UK*

November 25, 2021

Abstract

Any experiment with climate models relies on a potentially large set of spatio-temporal boundary conditions. These can represent both the initial state of the system and/or forcings driving the model output throughout the experiment. Whilst these boundary conditions are typically fixed using available reconstructions in climate modelling studies, they are highly uncertain, that uncertainty is unquantified, and the effect on the output of the experiment can be considerable. We develop efficient quantification of these uncertainties that combines relevant data from multiple models and observations. Starting from the coexchangeability model, we develop a coexchangeable process model to capture multiple correlated spatio-temporal fields of variables. We demonstrate that further exchangeability judgements over the parameters within this representation lead to a Bayes linear analogy of a hierarchical model. We use the framework to provide a joint reconstruction of sea-surface temperature and sea-ice concentration boundary conditions at the last glacial maximum (19-23 ka) and use it to force an ensemble of ice-sheet simulations using the FAMOUS-Ice coupled atmosphere and ice-sheet model. We demonstrate that existing boundary conditions typically used in these experiments are implausible given our uncertainties and demonstrate the impact of using more plausible boundary conditions on ice-sheet simulation.

Keywords: Bayes linear methods, exchangeability analysis, multi model ensemble

1 Introduction

Numerical experiments are vital tools to climate science. Knowledge of physical processes is embedded into software to simulate large scale events that are otherwise impossible to observe at the required spatial and temporal resolutions. The overwhelming majority of numerical climate simulators utilise boundary conditions to represent non-calculated physical processes on which the simulator relies. Generally, boundary conditions are fixed using a reference run or runs from existing multi-model ensembles (MMEs) that explicitly model the boundary condition’s physical process. For example, to run an ice-sheet model over the last glacial maximum (LGM) requires historical climate variables such as temperature, and precipitation (Gregoire et al., 2012) that can be obtained using the Paleoclimate Model Intercomparison Project (PMIP) ensemble of paleo-climate model runs (Ivanovic et al., 2016). MMEs can be biased and do not necessarily span the uncertainty of the physical process.

Some effort has been made to statistically reconstruct boundary conditions for computer models. Salter et al. (2018) use 16 realisations from a single model to develop a basis representation of a single spatio-temporal boundary condition that could be sampled from and calibrated. However, in terms of the fields that could be represented, this method was limited by the span of the ensemble. Liu and Guillas (2017) capture a 3200 dimensional bathymetry boundary condition for a Tsunami model using a dimension reduced kernel approximation to an SPDE model that is trained using a large data set of ship measurements. Whilst such approaches are attractive, they require a great deal of data to accurately capture the boundary conditions, and these data are not always available.

If modelling boundary conditions is viewed as a statistical reconstruction problem, there is a rich literature in statistics that attempts to combine data from multiple models and historical observations to infer spatio-temporal climate properties. Rougier et al. (2013) present a generalised framework, therein termed the coexchangeable model, where exchangeability judgements over an MME along with an assumption that each model in the ensemble has the same a priori covariance with the field they aim to represent lead to a simple model that can be used to estimate a true unobserved process. Second order inference via Bayes linear methods (Goldstein and Wooff, 2007) for this model ensures scalable reconstructions for a spatio-temporal field, and the requirement for only prior means and variances implies an easier prior modelling task. The coexchangeable model has seen some interest in more recent research, such as in Sansom et al. (2021) where it is used to model emergent constraints for future climate projections. Alternative to the methodology of Rougier et al. (2013), a line of research stemming from Chandler (2013) proposes a similar fully probabilistic model with individual weightings of each simulator rather than via an assumption of exchangeability. As noted in Rougier et al. (2013), the model in Chandler (2013) is a special case of the coexchangeable model.

Joint reconstruction of two or more physically distinct fields may, from a theoretical perspective, appear straightforward within hierarchical Bayesian frameworks such as those proposed by Chandler (2013). However, scalability becomes a much bigger challenge. This

is particularly so when the fields are highly dependent, as many in climate are. In this study we jointly model sea-surface temperature (SST) and sea-ice concentration (SIC) to drive a coupled atmosphere and ice-sheet model (we introduce this further in Section 4), where the dependence between the boundary conditions is critically important. The need for scalable inference and generality makes a coexchangeable approach desirable, and thus we develop a hierarchical coexchangeable model that offers a Bayes linear analogy to the natural Bayesian hierarchical model for the problem. From simple and natural exchangeability judgements, we develop efficient, scalable inference for joint reconstruction. This article proceeds as follows. Section 2 reviews the existing statistical literature on Bayes linear statistics and exchangeability analysis. Section 3 extends the coexchangeable model for coupled processes, providing a Bayes linear analogy to the Bayesian hierarchical model for which we then present scalable inference via geometric updating. Section 4 introduces our application to reconstructing SST and SIC using our methodology. Section 5 discusses the results of using the reconstructions of SST and SIC to simulate ice sheet-atmosphere interactions at the LGM, and Section 6 concludes. Code and data are provided as part of an R package downloadable from github.com/astfalckl/exanalysis.

2 Review of statistical methodology

2.1 Bayes Linear Theory

Recent discourse increasingly acknowledges the difficulty of specifying probability distributions to define likelihoods and prior beliefs for Bayesian analyses (Barthelmé and Chopin, 2014; Bissiri et al., 2016; Jesus and Chandler, 2011). This is especially relevant in climate applications where our quantities of interest are large spatio-temporal fields for which data may be (relatively) sparse. An alternative view treats expectation (rather than probability) as the primitive quantity (De Finetti, 1975). Under expectation as primitive, probabilities are the expectations of indicator functions for events. This motivates second-order approaches such as Bayes linear methods (see below and Goldstein and Wooff (2007)), where inference concerns expectations and variances directly rather than as a by-product of probabilistic inference.

Under the Bayes linear paradigm, beliefs on random quantities are described via expectations and variances which are then *adjusted* by data. Consider random quantity, X , with observations X_i , defined on the Hilbert space $\mathcal{X} = \sum_i h_i X_i$ for $X_i \in \mathcal{X} \subseteq \mathbb{R}^n$ and $h_i \in \mathbb{R}$, endowed with inner product $\langle X, Y \rangle = \mathbb{E}[X^\top Y]$. Denote by D the collection of observed data, $D = (X_1, \dots, X_m)$, and subspace \mathcal{D} as $\mathcal{D} = \text{span}[1, D]$. The adjusted expectation (written in terms of X and D as $\mathbb{E}_D[X]$, that is, the expectation of our beliefs X adjusted by data D) is the element in \mathcal{D} that minimises $\|X - \mathbb{E}_D[X]\|$. The adjusted expectation has solution

$$\mathbb{E}_D[X] = \mathbb{E}[X] + \text{cov}[X, D] \text{var}[D]^\dagger (D - \mathbb{E}[D]) \quad (1)$$

where $\text{var}[D]^\dagger$ is any pseudo-inverse of $\text{var}[D]$, most commonly the Moore-Penrose inverse. Equation (1) describes the orthogonal projection of each element of our beliefs, X , onto \mathcal{D} .

The adjusted variance, $\text{var}_D[X]$, is the outer product $\mathbb{E}[(X - \mathbb{E}_D[X])(X - \mathbb{E}_D[X])^\top]$ given $\mathbb{E}_D[X]$ in (1) and is

$$\text{var}_D[X] = \text{var}[X] - \text{cov}[X, D]\text{var}[D]^\dagger \text{cov}[D, X]. \quad (2)$$

Derivations of (1) and (2) are found in Sections 12.4 and 12.5 of Goldstein and Wooff (2007).

2.1.1 Bayes linear analysis of exchangeable data

Exchangeability for a sequence of random quantities within a probabilistic Bayesian analysis represents a simple symmetry judgement that implies that any finite sub-collection of quantities within the sequence have the same distribution (a priori). Second-order exchangeability for such a sequence is a similar analogue for judgements when expectation is primitive, and implies that each element of the same sequence has the same (prior) expectation and variance and that all pairs have the same covariance. If data, D , are second-order exchangeable we may, according to the second-order representation theorem (Goldstein, 1986), write

$$X_i = \mathcal{M}(X) + \mathcal{R}_i(X) \quad (3)$$

for a common mean $\mathcal{M}(X)$ and uncorrelated residuals $\mathcal{R}_i(X)$. Second-order exchangeability implies $\text{cov}[X_i, X_{i'}] = \Psi + \mathbf{1}_{i=i'}\Gamma \ \forall i, i'$. For second-order exchangeable sequences there is predictive sufficiency for updating beliefs on X by only updating $\mathcal{M}(X)$ by the data D . Mathematically we write this as $[D \perp\!\!\!\perp X]/\mathcal{M}(X)$, i.e., given $\mathcal{M}(X)$, D and X are uncorrelated. Further, the sample mean, $\bar{X} = \frac{1}{m} \sum_{i=1}^m X_i$, is Bayes linear sufficient for updating beliefs on $\mathcal{M}(X)$ (and consequently on X): $[D \perp\!\!\!\perp \mathcal{M}(X)]/\bar{X}$. A proof of Bayes linear sufficiency for exchangeable data is provided in Section 6.10 of Goldstein and Wooff (2007).

2.2 Exchangeability analysis for multi-model ensembles

We now review the coexchangeable model of Rougier et al. (2013) who use a Bayes linear approach to describe MMEs as follows. Let $\mathbb{X} := \{\mathbf{X}_1, \dots, \mathbf{X}_m\}$ be a collection of q -dimensional outputs from the m simulators that form the MME; \mathbf{X}^* , the true unobserved process that the simulators aim to model; and $\mathbf{Z}_\mathbf{X}$, the noisy and incomplete measurement of \mathbf{X}^* in the real world. The model requires only two assumptions: first, that the \mathbf{X}_i are second-order exchangeable and, second, that the \mathbf{X}_i are coexchangeable with the truth \mathbf{X}^* , implying $\text{cov}[\mathbf{X}^*, \mathbf{X}_i] = \Sigma, \ \forall i$.

As in (3), exchangeability within \mathbb{X} implies

$$\mathbf{X}_i = \mathcal{M}(\mathbf{X}) + \mathcal{R}_i(\mathbf{X}), \quad i = 1, \dots, m, \quad (4)$$

where $\mathcal{M}(\mathbf{X})$ is a shared mean term, the $\mathcal{R}_i(\mathbf{X})$ are the zero-mean, uncorrelated residuals of each simulator with common variance, and the $\mathcal{M}(\mathbf{X})$ and $\mathcal{R}_i(\mathbf{X})$ are uncorrelated. Coexchangeability between \mathbf{X}^* and \mathbb{X} implies sufficiency of $\mathcal{M}(\mathbf{X})$ for \mathbf{X}^* , $[\mathbf{X}_i \perp\!\!\!\perp \mathbf{X}^*]/\mathcal{M}(\mathbf{X}) \ \forall i$.

This allows us to write

$$\mathbf{X}^* = \mathbf{A}\mathcal{M}(\mathbf{X}) + \mathbf{U}_{\mathbf{X}} \quad (5)$$

where \mathbf{A} is a known matrix, and $\mathbf{U}_{\mathbf{X}}$ represents the ensemble discrepancy that is uncorrelated with $\mathcal{M}(\mathbf{X})$ and the $\mathcal{R}_i(\mathbf{X})$. The data, $\mathbf{Z}_{\mathbf{X}}$ are modelled as

$$\mathbf{Z}_{\mathbf{X}} = \mathbf{H}_{\mathbf{X}}\mathbf{X}^* + \mathbf{W}_{\mathbf{X}} \quad (6)$$

for measurement error $\mathbf{W}_{\mathbf{X}}$, and known incidence matrix $\mathbf{H}_{\mathbf{X}}$. The statistical model defined by (4)–(6) will hereafter be referred to as the “coexchangeable model”. Inference for this model makes use of Bayes linear sufficiency of the ensemble mean, $\bar{\mathbf{X}} = \frac{1}{m} \sum_{i=1}^m \mathbf{X}_i$, for updating by \mathbb{X} and is therefore very efficient. We outline the inferential procedure developed by Rougier et al. (2013) in the supplementary material.

3 The coexchangeable process model

Now consider each simulator as producing output pairs of q -dimensional fields $(\mathbf{X}_i, \mathbf{Y}_i)$ for $i = 1, \dots, m$, with the corresponding fields in reality denoted $(\mathbf{X}^*, \mathbf{Y}^*)$, for which we have (partial) observations $\mathbf{Z}_{\mathbf{X}}$ and $\mathbf{Z}_{\mathbf{Y}}$, made with some error. Whilst it is possible to consider the coexchangeable model over both fields simultaneously, a probabilistic Bayesian approach would normally leverage conditional probability laws to capture structured dependencies between the fields (these are a direct consequence of certain exchangeability judgements as with Sansom et al. (2021)). In what follows we capture explicit structural dependencies between random quantities (\mathbf{X}, \mathbf{Y}) , by first only imposing the coexchangeable model for $\mathbf{X}_i, \mathbf{X}^*$, and then considering exchangeability judgements over the processes $\mathbf{Y}_i(\mathbf{X}_i)$ and coexchangeability of $\mathbf{Y}^*(\mathbf{X}^*)$.

The rest of this section develops theory and methodology to model the random process $\mathbf{Y}(\mathbf{X})$ within a coexchangeability framework. Section 3.1 develops a general theory for second order exchangeable processes as a Bayes linear analogy to a Bayesian hierarchical model. Section 3.2 exploits the underlying geometry induced by the exchangeability for efficient updating. Finally, Section 3.3 develops our coexchangeable process model for the stated problem and gives results for efficient inference.

3.1 Exchangeable processes

Assume we observe a sequence of observation/covariate pairings from group i , $(Y_{i,1}, X_{i,1}), (Y_{i,2}, X_{i,2}), \dots$. Here we consider each simulator in our MME to comprise one such group and for the $(Y_{i,j}, X_{i,j})$ to be some p -dimensional sub-level process contained in $(\mathbf{Y}_i, \mathbf{X}_i)$. To help fix ideas, in the application in Section 4, \mathbf{Y}_i is spatio-temporal SIC and \mathbf{X}_i is spatio-temporal SST, both for simulator i . Each j indexes time (so that the $Y_{i,j}$ and $X_{i,j}$ are spatial processes), though it could instead index space, both space and time, or some other feature of the process. We impose conditional second order exchangeability within each group, the second order equivalent of the exchangeability judgements used in Bayesian

regression (see Williamson and Sansom, 2019, for discussion). Specifically, conditional second order exchangeability implies that the $Y_{i,1}, Y_{i,2}, \dots$ are second order exchangeable given fixed $X_{i,j} = X_i \forall j$. We may thus specify a mean process, $\mathbb{E}[Y_{i,j}(X_{i,j})] = \mathcal{M}(X_{i,j}, \beta_i) \in \mathbb{R}^p$ for some known covariate $X_{i,j}$ and unknown parameter $\beta_i \in \mathbb{R}^k$ specific to group i . According to the second order representation theorem,

$$Y_{i,j}(X_{i,j}) = \mathcal{M}(X_{i,j}, \beta_i) + \mathcal{R}_{i,j}(Y_{i,j}; X_{i,j}) \quad (7)$$

and $\text{cov}[Y_{i,j}(X_{i,j}), Y_{i,j'}(X_{i,j'})] = \text{cov}[\mathcal{M}(X_{i,j}, \beta_i), \mathcal{M}(X_{i,j'}, \beta_i)] + \mathbf{1}_{\{j=j'\}} \text{var}[\mathcal{R}_{i,j}(Y_{i,j}; X_{i,j})]$. $\mathcal{M}(X_{i,j}, \beta_i)$ may represent any functional relationship between $X_{i,j}$ and β_i and, to infer β_i from $Y_{i,j}(X_{i,j})$, we need only specify a joint inner product space in which they reside. We set

$$Y_{i,j}(X_{i,j}) = \phi(X_{i,j})\beta_i + \mathcal{R}_{i,j}(Y_{i,j}; X_{i,j}) \quad (8)$$

where $\phi(X_{i,j})$ is a matrix with k columns representing known basis functions of $X_{i,j}$. The choice to model $\mathcal{M}(X_{i,j}, \beta_i)$ linear in β_i is not required by the theory but it allows for natural specification of the inner product space and leads to sufficiency arguments (discussed below) that aid computation. To complete the analogy with a Bayesian hierarchical model, we impose second order exchangeability over the random vectors β_1, β_2, \dots so that

$$\beta_i = \mathcal{M}(\beta) + \mathcal{R}_i(\beta), \quad (9)$$

with expectation $\mathbb{E}[\beta_i] = \mathcal{M}(\beta)$ and covariance $\text{cov}[\beta_i, \beta_{i'}] = \text{cov}[\mathcal{M}(\beta_i), \mathcal{M}(\beta_{i'})] + \mathbf{1}_{\{i=i'\}} \text{var}[\mathcal{R}_i(\beta)]$, by the representation theorem.

Observe that $\mathbf{Y}_i = (Y_{i,1}(X_{i,1})^\top, \dots, Y_{i,n}(X_{i,n})^\top)^\top$ and $\mathbf{X}_i = (X_{i,1}^\top, \dots, X_{i,n}^\top)^\top$ for $j \in \{1, \dots, n\}$, and define $\Phi_i := \phi(\mathbf{X}_i)$, and $\mathcal{R}_i(\mathbf{Y}_i; \mathbf{X}_i) := (\mathcal{R}_{i,1}(Y_{i,1}; X_{i,1})^\top, \dots, \mathcal{R}_{i,n}(Y_{i,n}; X_{i,n})^\top)^\top$. We make additional natural belief specifications, $\text{cov}[\mathcal{R}_i(\mathbf{Y}_i; \mathbf{X}_i), \mathcal{R}_{i'}(\beta)] = 0$, and $\text{cov}[\mathcal{R}_i(\mathbf{Y}_i; \mathbf{X}_i), \mathcal{M}(\beta)] = 0 \forall i, i'$, and further note that $\text{cov}[Y_{i,j}(X_{i,j}), \beta_{i'}] = \phi(X_{i,j})\text{cov}[\beta_i, \beta_{i'}]$ results from our exchangeability judgements. Equations (8) and (9) imply

$$\begin{bmatrix} \mathbf{Y}_1 \\ \vdots \\ \mathbf{Y}_m \\ \beta_1 \\ \vdots \\ \beta_m \end{bmatrix} = \left[\begin{array}{ccc|c} \Phi_1 & \cdots & \mathbf{0}_{q \times k} & \\ \vdots & \ddots & \vdots & \mathbf{0}_{qm \times k} \\ \mathbf{0}_{q \times k} & \cdots & \Phi_m & \\ \hline \mathbf{0}_{km \times km} & & & \mathbf{J}_{m \times 1} \otimes \mathbf{I}_k \end{array} \right] \begin{bmatrix} \beta_1 \\ \vdots \\ \beta_m \\ \mathcal{M}(\beta) \end{bmatrix} + \begin{bmatrix} \mathcal{R}_1(\mathbf{Y}_1; \mathbf{X}_1) \\ \vdots \\ \mathcal{R}_m(\mathbf{Y}_m; \mathbf{X}_m) \\ \mathcal{R}_1(\beta) \\ \vdots \\ \mathcal{R}_m(\beta) \end{bmatrix}, \quad (10)$$

where $\mathbf{0}_{a \times b}$ is a $a \times b$ zero matrix, $\mathbf{J}_{a \times b}$ is a $a \times b$ matrix of ones, and \mathbf{I}_a is the $a \times a$ identity matrix.

We note that the specification of (10) differs from the standard approach to modelling exchangeable processes in Bayes linear statistics where inference only concerns $\mathcal{M}(\beta)$ by, in effect, substituting (9) into (8) (see Goldstein and Wooff (1998)). By jointly modelling the β_i and $\mathcal{M}(\beta)$ we provide a closer analogy to Bayesian hierarchical models. Advantages of (10) are that group level inference on the β_i are available, and our adjusted beliefs are subject to the same types of shrinkage effects seen in Bayesian hierarchical models (for instance, see Section 8.4.2 of Hoff (2009)). In the context of climate modelling, revised beliefs of the β_i provide inference on the physical processes at the model level.

3.2 Inference for exchangeable processes

Noting that (9) is equivalently restated as $0 = \mathcal{M}(\beta) + \mathcal{R}_j(\beta) - \beta_j$, and using the re-parametrisation of Hodges (1998), we can re-express (10) via

$$\begin{bmatrix} \mathbf{Y}_1 \\ \vdots \\ \mathbf{Y}_m \\ \mathbf{0}_{km \times 1} \end{bmatrix} = \left[\begin{array}{ccc|c} \Phi_1 & \cdots & \mathbf{0}_{q \times k} & \\ \vdots & \ddots & \vdots & \mathbf{0}_{qm \times k} \\ \mathbf{0}_{q \times k} & \cdots & \Phi_m & \\ \hline & & -\mathbf{I}_{km} & \mathbf{J}_{m \times 1} \otimes \mathbf{I}_k \end{array} \right] \begin{bmatrix} \beta_1 \\ \vdots \\ \beta_m \\ \mathcal{M}(\beta) \end{bmatrix} + \begin{bmatrix} \mathcal{R}_1(\mathbf{Y}_1; \mathbf{X}_1) \\ \vdots \\ \mathcal{R}_m(\mathbf{Y}_m; \mathbf{X}_m) \\ \mathcal{R}_1(\beta) \\ \vdots \\ \mathcal{R}_m(\beta) \end{bmatrix} \quad (11)$$

with the familiar linear canonical form $\mathbf{Y} = \mathbf{XB} + \mathbf{E}$. As we consider the joint representation, expectation is taken jointly over \mathbf{Y}_i and β_i . Belief specifications follow from Section 3.1 and the adjusted expectation, $\mathbb{E}_{\mathbf{Y}}[\mathbf{B}]$, and adjusted variance, $\text{var}_{\mathbf{Y}}[\mathbf{B}]$, are calculated via (1) and (2); the joint belief specifications and specific updating equations are provided in the supplementary material.

Calculating $\mathbb{E}_{\mathbf{Y}}[\mathbf{B}]$ and $\text{var}_{\mathbf{Y}}[\mathbf{B}]$ requires the inversion of the $m(q+k) \times m(q+k)$ matrix, $\text{var}[\mathbf{Y}]$. We show in Theorem 3.1 (below) that a Bayes linear sufficiency argument can be made to make equivalent inference for \mathbf{B} instead with the inversion of a smaller (when $k < q$) $2km \times 2km$ matrix. For climate models, q is generally large as either the size of the process, p , is large (such as when $Y_{i,j}$ is a high-resolution spatial process), or n is large (such as when j indexes space and/or time). For many basis designs $k \ll q$, and when groups, i , index MIP simulations, m is generally small (our application has $m = 13$).

Theorem 3.1. *Let $\hat{\beta} = (\hat{\beta}_1, \dots, \hat{\beta}_m)$ with $\hat{\beta}_i = (\Phi_i^\top \Phi_i)^\dagger \Phi_i^\top \mathbf{Y}_i$. Then $\hat{\beta}$ is Bayes linear sufficient for \mathbf{Y} for adjusting \mathbf{B} if the column space of projection matrix $P_i = \Phi_i(\Phi_i^\top \Phi_i)^\dagger \Phi_i^\top$, $C(P_i)$, is invariant over i , i.e., $C(P_i) = \mathcal{C} \forall i$.*

Proof. As P_i is a projection matrix (this is immediately verified as $P_i^2 = P_i$), $\hat{\mathbf{Y}}_i = P_i \mathbf{Y}_i \in C(P_i)$ projects \mathbf{Y}_i into the column space of P_i and $\hat{R}_i = \mathbf{Y}_i - \hat{\mathbf{Y}}_i = (1 - P_i)\mathbf{Y}_i \in N(P_i)$ projects \mathbf{Y}_i into the null space of P_i , $N(P_i)$. Define \mathcal{Y}_i as the inner product space in which \mathbf{Y}_i resides and on which P_i is defined. \mathcal{Y}_i may be partitioned as direct sum $\mathcal{Y}_i = C(P_i) \oplus N(P_i)$. As $C(P_i)$ and $N(P_i)$ form orthogonal subspaces, $\langle A, B \rangle_{\mathcal{Y}_i} = 0$ and so $\text{cov}[A, B] = 0$ for any vector $A \in C(P_i)$ and $B \in N(P_i)$.

From (11), the conditions $[\mathbf{Y}_i \perp\!\!\!\perp \mathcal{M}(\beta)]/\hat{\beta}_i$ and $[\mathbf{Y}_i \perp\!\!\!\perp \beta_{i'}]/\hat{\beta}_i \forall i, i'$ satisfy Bayes linear sufficiency, $[\mathbf{Y} \perp\!\!\!\perp \mathbf{B}]/\hat{\beta}$. From Theorem 5.20.7 Goldstein and Wooff (2007), $[\mathbf{Y}_i \perp\!\!\!\perp \mathcal{M}(\beta)]/\hat{\beta}_i$ and $[\mathbf{Y}_i \perp\!\!\!\perp \beta_{i'}]/\hat{\beta}_i \forall i, i'$ are satisfied if $\text{cov}[\mathbf{Y}_i - \mathbb{E}_{\hat{\beta}_i}[\mathbf{Y}_i], \mathcal{M}(\beta)] = 0$ and $\text{cov}[\mathbf{Y}_i - \mathbb{E}_{\hat{\beta}_i}[\mathbf{Y}_i], \beta_{i'}] = 0$, respectively. Observe that $\text{cov}[\mathbf{Y}_i, \hat{\mathbf{Y}}_{i'}] = \text{cov}[P_i \mathbf{Y}_i + (1 - P_i)\mathbf{Y}_i, \hat{\mathbf{Y}}_{i'}] = \text{cov}[\hat{\mathbf{Y}}_i, \hat{\mathbf{Y}}_{i'}] \forall i, i'$ so that $\text{cov}[\mathbf{Y}_i, \hat{\beta}_{i'}] = \Phi_i \text{cov}[\hat{\beta}_i, \hat{\beta}_{i'}] \forall i, i'$ and thus calculating $\mathbb{E}_{\hat{\beta}_i}[\mathbf{Y}_i]$ via (1) yields $\mathbb{E}_{\hat{\beta}_i}[\mathbf{Y}_i] = \Phi_i \hat{\beta}_i = \hat{\mathbf{Y}}_i$. If $C(P_i)$ and $N(P_i)$ are invariant over i (i.e., $C(P_i) = \mathcal{C}$ and $N(P_i) = \mathcal{N}$) then $C(P_i) \perp\!\!\!\perp N(P_{i'}) \forall i, i'$. Thus $\mathbf{Y}_i - \hat{\mathbf{Y}}_i \in \mathcal{N}$ and $\Phi_i \beta_i, \Phi_i \mathcal{M}(\beta) \in \mathcal{C}$, $\forall i$, so that $\text{cov}[\mathbf{Y}_i - \mathbb{E}_{\hat{\beta}_i}[\mathbf{Y}_i], \Phi_i \mathcal{M}(\beta)] = 0$ and $\text{cov}[\mathbf{Y}_i - \mathbb{E}_{\hat{\beta}_i}[\mathbf{Y}_i], \Phi_i \beta_{i'}] = 0 \forall i, i'$, and thus $\text{cov}[\mathbf{Y}_i - \mathbb{E}_{\hat{\beta}_i}[\mathbf{Y}_i], \mathcal{M}(\beta)] = 0$ and $\text{cov}[\mathbf{Y}_i - \mathbb{E}_{\hat{\beta}_i}[\mathbf{Y}_i], \beta_{i'}] = 0 \forall i, i'$. \square

As $C(P_i) = C(\Phi_i)$, if Φ_i is full rank this is sufficient (but not necessary) in satisfying the condition $C(P_i) = \mathcal{C} \forall i$ in Theorem 3.1 — most sensible basis designs will ensure this. Assuming $C(P_i) = \mathcal{C} \forall i$, and appealing to the sufficiency of $\hat{\beta}$ for \mathbf{Y} for adjusting \mathbf{B} , we write the joint specification of the exchangeability judgements made in Section 3.1 as

$$\begin{bmatrix} \hat{\beta}_1 \\ \vdots \\ \hat{\beta}_m \\ \mathbf{0}_{km \times 1} \end{bmatrix} = \left[\begin{array}{c|c} \mathbf{I}_{km} & \mathbf{0}_{km \times k} \\ \hline -\mathbf{I}_{km} & \mathbf{J}_{m \times 1} \otimes \mathbf{I}_k \end{array} \right] \begin{bmatrix} \beta_1 \\ \vdots \\ \beta_m \\ \mathcal{M}(\beta) \end{bmatrix} + \begin{bmatrix} \mathcal{R}_1(\hat{\beta}; \mathbf{X}_1) \\ \vdots \\ \mathcal{R}_m(\hat{\beta}; \mathbf{X}_m) \\ \mathcal{R}_1(\beta) \\ \vdots \\ \mathcal{R}_m(\beta) \end{bmatrix} \quad (12)$$

where $\mathcal{R}_i(\hat{\beta}; \mathbf{X}_i) = (\Phi_i^\top \Phi_i)^\dagger \Phi_i^\top \mathcal{R}_i(\mathbf{Y}_i; \mathbf{X}_i)$. Calculation of $\mathbb{E}_{\hat{\beta}}[\mathbf{B}]$ and $\text{var}_{\hat{\beta}}[\mathbf{B}]$ follows (1) and (2); the specific equations are given in the supplementary material. If interest lies only in the belief updates of $\mathcal{M}(\beta)$, then computation of $\mathbb{E}_{\hat{\beta}}[\mathcal{M}(\beta)]$ and $\text{var}_{\hat{\beta}}[\mathcal{M}(\beta)]$ exist by only computing the requisite parts of $\mathbb{E}_{\hat{\beta}}[\mathbf{B}]$ and $\text{var}_{\hat{\beta}}[\mathbf{B}]$; equations for $\mathbb{E}_{\hat{\beta}}[\mathcal{M}(\beta)]$ and $\text{var}_{\hat{\beta}}[\mathcal{M}(\beta)]$ are also provided in the supplementary material.

3.3 Reality as a coexchangeable process

We now show how judgements of coexchangeability may be made to incorporate (11) or (12) into the coexchangeable model. Define the true process of \mathbf{Y}_i that the simulators attempt to resolve given some \mathbf{X}^* as $\mathbf{Y}^*(\mathbf{X}^*)$. We impose coexchangeability of $\mathbf{Y}^*(\mathbf{X}^*)$ and \mathbf{Y}_i given fixed $\mathbf{X}_i = \mathbf{X}$ (and hence $\Phi_i = \Phi$) $\forall i$, i.e., $\text{cov}[\mathbf{Y}^*(\mathbf{X}^*), \mathbf{Y}_i] = \Sigma(\mathbf{X}^*) \forall i$. As $\text{cov}[\mathbf{Y}^*(\mathbf{X}^*), \mathbf{Y}_i] = \text{cov}[\mathbf{Y}^*(\mathbf{X}^*), \Phi \beta_i] = \Sigma(\mathbf{X}^*) = \Gamma(\mathbf{X}^*) \Phi^\top$ we find that $\text{cov}[\mathbf{Y}^*(\mathbf{X}^*), \beta_i] = \Gamma(\mathbf{X}^*) \forall i$ and so we have coexchangeability of $\mathbf{Y}^*(\mathbf{X}^*)$ and β_i . Bayes linear sufficiency of $\mathcal{M}(\beta)$ for the \mathbf{Y}_i for adjusting $\mathbf{Y}^*(\mathbf{X}^*)$ follows. We write a model for $\mathbf{Y}^*(\mathbf{X}^*)$ such that

$$\mathbf{Y}^*(\mathbf{X}^*) = A(\mathbf{X}^*) \mathcal{M}(\beta) + \mathbf{U}_{\mathbf{Y}}, \quad (13)$$

where $\mathbf{U}_{\mathbf{Y}}$ is a model-mismatch term orthogonal to the \mathbf{Y}_i and the assumption of coexchangeability permits $A(\mathbf{X}^*)$ to be any matrix of suitable dimensions. The choice of $A(\mathbf{X}^*) = \phi(\mathbf{X}^*)$ is logical in our context as an analogue to (8) for the reality model, but different choices are permissible should they make sense to the application. Finally, the data, $\mathbf{Z}_{\mathbf{Y}}$ are modelled as

$$\mathbf{Z}_{\mathbf{Y}} = \mathbf{H}_{\mathbf{Y}} \mathbf{Y}^*(\mathbf{X}^*) + \mathbf{W}_{\mathbf{Y}}, \quad (14)$$

for measurement error $\mathbf{W}_{\mathbf{Y}}$, and known incidence matrix $\mathbf{H}_{\mathbf{Y}}$.

Similar to Rougier et al. (2013), we assume sufficiency of $\mathbf{Y}^*(\mathbf{X}^*)$ for $\mathbf{Z}_{\mathbf{Y}}$, allowing us to update beliefs on $\mathbf{Y}^*(\mathbf{X}^*)$ in two stages. As adjusted expectation is a linear operator (Property 3.2.1 Goldstein and Wooff (2007)), $\mathbf{U}_{\mathbf{Y}}$ is defined uncorrelated with the ensemble, and supposing the conditions of Theorem 3.1 hold, the adjustments of $\mathbf{Y}^*(\mathbf{X}^*)$ by the

$(\mathbf{Y}_i, \mathbf{X}_i)$ are

$$\mathbb{E}_{(\mathbf{Y}, \mathbf{X})}[\mathbf{Y}^*(\mathbf{X}^*)] = \mathbb{E}_{\hat{\beta}}[\mathbf{Y}^*(\mathbf{X}^*)] = \phi(\mathbf{X}^*)\mathbb{E}_{\hat{\beta}}[\mathcal{M}(\beta)] + \mathbb{E}[\mathbf{U}_{\mathbf{Y}}], \text{ and} \quad (15)$$

$$\text{var}_{(\mathbf{Y}, \mathbf{X})}[\mathbf{Y}^*(\mathbf{X}^*)] = \text{var}_{\hat{\beta}}[\mathbf{Y}^*(\mathbf{X}^*)] = \phi(\mathbf{X}^*)\text{var}_{\hat{\beta}}[\mathcal{M}(\beta)]\phi(\mathbf{X}^*)^\top + \text{var}[\mathbf{U}_{\mathbf{Y}}]. \quad (16)$$

Note that if the conditions of Theorem 3.1 are not met, then the first equality is not necessarily true and the adjustments on the right hand side of these equations would be with respect to (\mathbf{Y}, \mathbf{X}) . The second update of $\mathbf{Y}^*(\mathbf{X}^*)$ by data $\mathbf{Z}_{\mathbf{Y}}$ is calculated as

$$\begin{aligned} \mathbb{E}_{\hat{\beta}, \mathbf{Z}_{\mathbf{Y}}}[\mathbf{Y}^*(\mathbf{X}^*)] &= \mathbb{E}_{\hat{\beta}}[\mathbf{Y}^*(\mathbf{X}^*)] + \text{var}_{\hat{\beta}}[\mathbf{Y}^*(\mathbf{X}^*)]\mathbf{H}_{\mathbf{Y}}^\top \\ &\quad (\mathbf{H}_{\mathbf{Y}}\text{var}_{\hat{\beta}}[\mathbf{Y}^*(\mathbf{X}^*)]\mathbf{H}_{\mathbf{Y}}^\top + \text{var}[\mathbf{W}_{\mathbf{Y}}])^{-1}(\mathbf{Z}_{\mathbf{Y}} - \mathbf{H}_{\mathbf{Y}}\mathbb{E}_{\hat{\beta}}[\mathbf{Y}^*(\mathbf{X}^*)]), \text{ and} \end{aligned} \quad (17)$$

$$\begin{aligned} \text{var}_{\hat{\beta}, \mathbf{Z}_{\mathbf{Y}}}[\mathbf{Y}^*(\mathbf{X}^*)] &= \text{var}_{\hat{\beta}}[\mathbf{Y}^*(\mathbf{X}^*)] - \text{var}_{\hat{\beta}}[\mathbf{Y}^*(\mathbf{X}^*)]\mathbf{H}_{\mathbf{Y}}^\top \\ &\quad (\mathbf{H}_{\mathbf{Y}}\text{var}_{\hat{\beta}}[\mathbf{Y}^*(\mathbf{X}^*)]\mathbf{H}_{\mathbf{Y}}^\top + \text{var}[\mathbf{W}_{\mathbf{Y}}])^{-1}\mathbf{H}_{\mathbf{Y}}\text{var}_{\hat{\beta}}[\mathbf{Y}^*(\mathbf{X}^*)]. \end{aligned} \quad (18)$$

4 Joint reconstruction of Paleo sea-surface temperature and sea-ice with PMIP3 and PMIP4

Our application is the joint reconstruction of SST and SIC in order to provide spatio-temporal boundary conditions for coupled ice sheet-atmosphere simulations. These simulations will be run with the FAMOUS-Ice simulator (Smith et al., 2021), a computationally efficient model which can represent ice sheet-climate processes in sufficient detail to accurately simulate the contemporary Greenland ice sheet (Gregory et al., 2020). One way to test the models' ability to simulate climate and ice sheets different from today (e.g. the future), is to simulate the past (Kageyama et al., 2017; Harrison et al., 2015; Schmidt et al., 2014). The deglaciation ($\sim 21,000$ to $7,000$ years ago) is the most natural period to study, given the relatively rich source of observations on the climate and ice sheets (compared to the more distant past), which respectively warmed and shrunk due to increasing greenhouse gas concentrations. To begin to study the deglaciation, an ice sheet needs to be "grown" within the model under the steady state boundary conditions (SST and SIC) of the relatively stable conditions of the LGM ($\sim 23,000$ to $19,000$ years ago). The character of the resulting ice sheets are sensitive to these boundary conditions and so it is crucial to use an accurate reconstruction, realistic uncertainty quantification and a method for perturbing the boundary conditions under uncertainty to force the ice sheet model.

Existing reconstructions of LGM SST and SIC include the Climate Long range Investigation, Mapping, and Prediction (CLIMAP) project (CLIMAP Project, 1981), the Glacial Atlantic Ocean Mapping (GLAMAP) project (Sarnthein et al., 2003), the Multiproxy Approach for the Reconstruction of the Glacial Ocean Surface (MARGO) project (Kucera et al., 2005), and more recently Paul et al. (2020). These global reconstructions (as well as other regionalised reconstructions such as De Vernal et al. (2005) and Gersonde et al. (2005)) are 'data only' based solely on paleodata syntheses and do not include numerical simulations in their analyses. As such, they are subject to large measurement error, large biases in polar regions, incomplete spatial coverage, and poor temporal resolution. Modern

statistical methods (e.g. in Zhang et al. (2020) and Sha et al. (2019)) for reconstructing spatio-temporal climate fields rely on computationally intensive methods that require large observational data and so are inappropriate here given the relative data sparsity at the LGM.

Coupled simulations of the LGM are useful to ensure spatio-temporal consistency of SST and SIC, but these can also be very different from observations in critical regions for growing ice sheets (Salter et al., 2019). Tierney et al. (2020) use a variant of the ensemble square-root Kalman filter (Whitaker and Hamill, 2002) to adjust a model with observations to provide SST reconstruction (with uncertainty quantification), based on the iCESM model. Differences in model physics are typically much wider across models than the variation of a particular model when varying its parameters (Masson and Knutti, 2011). Therefore, reconstructions based on a single model may be biased and overconfident. PMIP defines experimental protocols for coupled ocean-atmosphere models (with prescribed greenhouse gases and ice sheets) to simulate the LGM climate (Kageyama et al., 2017, 2021). The PMIP community has produced MMEs for different phases of the project; PMIP2, PMIP3, PMIP4 run with different generations of model and slight adjustments in input greenhouse gases and ice sheets. Annan and Hargreaves (2013) made use of such MMEs to produce an SST reconstruction by regressing the proxy data to the PMIP2 model data. Other uses of PMIP data have been to directly force ice sheet simulations (Gregoire et al., 2016).

Our methodology allows for the first joint reconstruction of SST and SIC (we are aware of) that coherently combines the PMIP models (we use PMIP3 and PMIP4) with available proxy data to deliver boundary conditions with uncertainty quantification. We also demonstrate inference for the differences in model physics that our Bayes linear analogy to the hierarchical model offers.

4.1 Numerical simulators and paleo-observations

4.1.1 The MME: PMIP global climate models

As with other exchangeable MME methods (Rougier et al., 2013; Sansom et al., 2021), we select a single representative simulation from each modelling group that contributed to the PMIP3 and PMIP4 MMEs (Kageyama et al., 2021), in order to make the assumption of prior exchangeability, and exchangeable processes, reasonable. However, for the HadCM3 model simulations, we make use of all three available PMIP4 simulations that use different ice sheet boundary conditions as these differences are known to affect the simulated SST and SIC. The $m = 13$ models selected were

$$S = \{\text{CNRM-3, IPSL-3, MIROC-3, MPI-3, CCSM4-3, GISS-3, MRI-3, AWI-4,} \\ \text{MIROC-4, MPI-4, HadCM3-PMIP, HadCM3-Glac1D, HadCM3-Ice6G}\}. \quad (19)$$

Each ensemble member was projected onto the FAMOUS ocean grid with $p = 4145$ spatial locations, and we use the 12 monthly means of SST and SIC. The choice to use monthly means rather than a full simulation is based on only having monthly means for 7 of the 13 ensemble members.

4.1.2 SST Observations

We use proxy temperature data, $\mathbf{Z}_{\mathbf{X}}$, obtained from sea-bed sediment core samples to infer LGM SST, \mathbf{X}^* . We use the MARGO compilation (Kucera et al., 2005) supplemented with some more recent data from Benz et al. (2016) to fill in some of the sparsity in the Southern Ocean. Most proxy temperature data measure SST as an annual mean, but Southern Ocean locations are provided as summer means. The measurements from final data compilation are shown in Figure 1, annual and summer means are depicted with points and triangles, respectively. Sea-ice extents are represented by a red dashed line. The Southern sea-ice extent is as reported in Gersonde et al. (2005) and the Northern sea-ice extent is provided by coauthors.

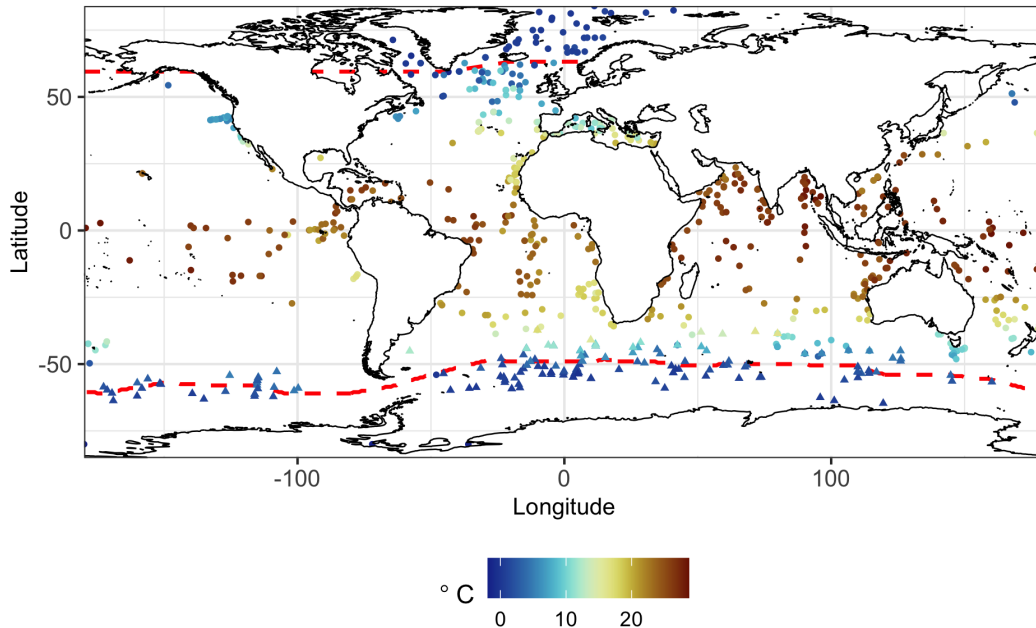


Figure 1: Proxy-based measurements of LGM SST and maximum sea-ice extents. Annual mean and summer mean sea-surface temperatures are represented by points and triangles, respectively. Sea-ice extents are represented by a red dashed line. The Southern sea-ice extent is as reported in Gersonde et al. (2005) and the Northern sea-ice extent is provided by coauthors.

There is very likely some strong observation bias in the foraminifera-based proxy measurements from the Arctic and Nordic seas, approximately north of 62° N. For example, in this region, very cold water and full sea-ice coverage are common; both inhospitable conditions for most foraminifera species. The non-existence of foraminifera in ocean sediments are rarely reported, since the absence of foraminifera leaves little to be analysed in ecological or geochemical studies. Thus, observations may be biased towards the warm climate events naturally present within the inter-decadal variability, when foraminifera are found. We account for this through specification of measurement error in (6), $\mathbf{W}_{\mathbf{X}}$. Define B_N as a set of indices that index observations from the Nordic Seas in $\mathbf{Z}_{\mathbf{X}}$. We set $\mathbb{E}[\mathbf{W}_{\mathbf{X}}]_b = 2$ and $\mathbb{E}[\mathbf{W}_{\mathbf{X}}]_{b^*} = 0$ for $b \in B_N$ and $b^* \notin B_N$. As the bias originates from a systematic reporting error we believe the measurement errors to be correlated. We partition

$\text{var}[\mathbf{W}_{\mathbf{X}}] = V_{\mathbf{D}}(\mathbf{I} + V_{\mathbf{B}})V_{\mathbf{D}}$ and set $V_{\mathbf{D}}$ as the diagonal matrix of the reported standard deviations in the MARGO dataset, and $V_{\mathbf{B}[b,b']} = 1 \forall b, b' \in B_N$ where $b \neq b'$, and 0 otherwise. Finally, we set incidence matrix in (6), $\mathbf{H}_{\mathbf{X}} = \mathbf{H}_{\mathbf{X}}^T \otimes \mathbf{H}_{\mathbf{X}}^S$, where $\mathbf{H}_{\mathbf{X}}^T$ calculates either the annual or summer means of \mathbf{X}^* as necessary, and $\mathbf{H}_{\mathbf{X}}^S$ spatially interpolates these averages from simulator's spatial grid to the data locations.

4.1.3 SIC Observations

Point-wise proxy measurements of SIC are difficult to interpret and unreliable. More robust are estimates of maximum (winter) sea-ice extent. The Northern and Southern extents used for $\mathbf{Z}_{\mathbf{Y}}$ are shown in Figure 1 by the red dashed lines. The Southern Hemisphere maximum sea-ice extent is as published in Gersonde et al. (2005). Northern Hemisphere extents are only available for specific regions (e.g. De Vernal et al. (2005); Crosta et al. (1998); Xiao et al. (2015)), so we use a simple estimate of the Northern Hemisphere sea-ice extent provided by our domain experts. We specify $\mathbf{Z}_{\mathbf{Y}}$ as a p -dimensional vector that records a 1 at spatial locations within the extent boundaries, and a 0 outside. Incidence matrix, $\mathbf{H}_{\mathbf{Y}}$ in (14) is a $p \times q$ matrix that collates, from $\mathbf{Y}^*(\mathbf{X}^*)$, the February SIC from the Northern hemisphere and August SIC from the Southern hemisphere. We specify measurement error, $\mathbf{W}_{\mathbf{Y}}$, to be spatially correlated and certain of SIC estimates in the poles (where we are confident that there is full sea-ice coverage) and mid-latitude and equatorial regions (where we are confident there is zero sea-ice). We set $\text{var}[\mathbf{W}_{\mathbf{Y}}] = K\text{cor}[\mathbf{W}_{\mathbf{Y}}]K$ where K is a diagonal matrix that represents our marginal uncertainty (capturing the fact that we are more uncertain of the coverage the nearer we get to the extent boundary) and $\text{cor}[\mathbf{W}_{\mathbf{Y}}]$ is spatially correlated error; descriptions of K and $\text{cor}[\mathbf{W}_{\mathbf{Y}}]$ are given in the supplementary material.

4.2 Fitting the coexchangeable process model

To fit the coexchangeable process model we first model SST via the coexchangeable model described in Section 2.2 and the process of SIC given SST is modelled using the methodology developed in Section 3.

4.2.1 Sea-surface temperature

Following notation in Section 2.2, define the ensemble SST's as $\mathbb{X} = \{\mathbf{X}_1, \dots, \mathbf{X}_m\}$, with each \mathbf{X}_i as a second order exchangeable vector of length $q = 12p$. This leads to the representation in equation (4), for which we require prior specification of $\text{var}[\mathcal{M}(\mathbf{X})]$ and $\text{var}[\mathcal{R}_i(\mathbf{X})]$. Coexchangeability of \mathbf{X}_i and \mathbf{X}^* leads to (5), for which we require prior specification of model mismatch terms $\mathbb{E}[\mathbf{U}_{\mathbf{X}}]$, $\text{var}[\mathbf{U}_{\mathbf{X}}]$ and incidence matrix \mathbf{A} . We specify $\text{var}[\mathcal{R}(\mathbf{X})] = \alpha^2 \text{var}[\mathcal{M}(\mathbf{X})]$ so that $\text{var}[\mathbf{X}] = (1 + \alpha^2)\text{var}[\mathcal{M}(\mathbf{X})]$ and, following Rougier et al. (2013), set $\mathbb{E}[\mathbf{U}_{\mathbf{X}}] = \mathbf{0}$ and $\mathbf{A} = \mathbf{I}$.

For SST (and most climate fields) we can exploit spatio-temporal structure so that computation of adjusted beliefs is scalable. The most obvious way to do this is to assume

separability through space and time so that $\text{var}[\mathbf{X}]$ and $\text{var}[\mathbf{X}^*]$ (and hence $\text{var}[\mathbf{U}_{\mathbf{X}}]$) have a Kronecker structure. For example, $\text{var}[\mathbf{X}] = \text{var}[\mathbf{X}_T] \otimes \text{var}[\mathbf{X}_S]$ where T denotes time and S denotes space. If we similarly partition $\text{var}[\mathbf{U}_{\mathbf{X}}] = \text{var}[\mathbf{U}_{\mathbf{X}_T}] \otimes \text{var}[\mathbf{U}_{\mathbf{X}_S}]$ and equate either $\text{var}[\mathbf{X}_T] = \text{var}[\mathbf{U}_{\mathbf{X}_T}]$ or $\text{var}[\mathbf{X}_S] = \text{var}[\mathbf{U}_{\mathbf{X}_S}]$ computation of our adjusted beliefs is efficient. Note that this assumption is far weaker than the application in Rougier et al. (2013) where it is simply assumed that $\kappa^2 \text{var}[\mathbf{X}] = \text{var}[\mathbf{U}]$. Here, we set $\text{var}[\mathbf{X}_T] = \text{var}[\mathbf{U}_{\mathbf{X}_T}] = \mathbf{J}_{n \times n}$ as our domain experts believe that discrepancies between the \mathbf{X}_i and reality are predominantly spatial and constant in time.

We set $\text{var}[\mathbf{X}_S]$ as the positive semi-definite matrix that minimises the distance between $\text{var}[\mathbf{X}]$ and the empirical covariance matrix of \mathbb{X} , $\mathbf{S}_{\mathbf{X}}$, under the Frobenius norm. This specification follows similar arguments to Rougier et al. (2013) where $\text{var}[\mathbf{X}] = \mathbf{S}_{\mathbf{X}}$, but preserves Kronecker structure in $\text{var}[\mathbf{X}]$ to allow for efficient computation. Details of this calculation are in the supplementary material. Elements of $\text{var}[\mathbf{U}_{\mathbf{X}_S}]$ are defined via the C^4 -Wendland covariance function such that

$$\text{var}[\mathbf{U}_{\mathbf{X}_S}]_{[s,s']} = \kappa^2 \left(1 + \tau \frac{d(s,s')}{c} + \frac{\tau^2 - 1}{3} \frac{d(s,s')^2}{c^2} \right) \left(1 - \frac{d(s,s')}{c} \right)_+^\tau \quad (20)$$

where $\tau \geq 6$, $c \in (0, \pi]$, $(a)_+ = \max(0, a)$, and $d(i, j)$ is the geodesic distance between locations i and j . The C^4 -Wendland covariance function is commonly chosen so as to define a smooth process on the sphere; (see, for example Astfalck et al., 2019). Parameters are specified as $\kappa^2 = 1.61$, $c = 0.92$, and $\tau = 6$; this represents the prior-beliefs of domain experts as to the behaviour of $\mathbf{U}_{\mathbf{X}}$.

The 2-stage Bayes linear update follows Rougier et al. (2013) and is given in the supplementary material. As with Rougier et al. (2013), we assume the first update $\mathbb{E}_{\bar{\mathbf{X}}}[\mathbf{X}^*]$ is well approximated by $\mathbb{E}_{\bar{\mathbf{X}}}[\mathbf{X}^*] \approx \bar{\mathbf{X}}$ and we calculate $\text{var}_{\bar{\mathbf{X}}}[\mathbf{X}^*] = \left(\frac{\alpha^2}{m + \alpha^2} \right) \text{var}[\mathcal{M}(\mathbf{X})] + \text{var}[\mathbf{U}_{\mathbf{X}}]$ so $\text{var}_{\bar{\mathbf{X}}}[\mathbf{X}^*] \rightarrow \text{var}[\mathbf{U}]$ as $m \rightarrow \infty$. Here, we choose $\alpha^2 = 1$ and have $m = 13$ and so do not assume $\text{var}_{\bar{\mathbf{X}}}[\mathbf{X}^*] \approx \text{var}[\mathbf{U}]$. From specifications $\text{var}[\mathbf{U}_{\mathbf{X}_T}] = \text{var}[\mathbf{X}_T]$ and $\text{var}[\mathbf{X}] = 2\text{var}[\mathcal{M}(\mathbf{X})]$, $\text{var}_{\bar{\mathbf{X}}}[\mathbf{X}^*]$ has Kronecker structure so that $\text{var}_{\bar{\mathbf{X}}}[\mathbf{X}^*] = \text{var}_{\bar{\mathbf{X}}}[\mathbf{X}_T^*] \otimes \text{var}_{\bar{\mathbf{X}}}[\mathbf{X}_S^*]$, where $\text{var}_{\bar{\mathbf{X}}}[\mathbf{X}_T^*] = \mathbf{J}_{n \times n}$ and $\text{var}_{\bar{\mathbf{X}}}[\mathbf{X}_S^*] = \frac{\text{var}[\mathbf{X}_S]}{2(m+1)} + \text{var}[\mathbf{U}_{\mathbf{X}_S}]$. The above specifications lead to a prior predictive for \mathbf{X}^* (prior to observing $\mathbf{Z}_{\mathbf{X}}$) that is warmer than our true beliefs at the poles (where we are certain there was full sea ice coverage and so the SST must be -1.92°C). This is problematic due to the data sparsity in the poles, and so we correct our prior by adding 10 equally spaced (over longitude) pseudo-observations at 80°N and 80°S , each of -1.92°C . Figures 2a and 2b plot $\mathbb{E}_{\bar{\mathbf{X}}}[\mathbf{X}^*]$ and marginal variance of $\text{var}_{\bar{\mathbf{X}}}[\mathbf{X}^*]$, respectively, for January.

The second update is calculated by

$$\mathbb{E}_{\bar{\mathbf{X}}, \mathbf{Z}_{\mathbf{X}}}[\mathbf{X}^*] = \bar{\mathbf{X}} + \text{var}_{\bar{\mathbf{X}}}[\mathbf{X}^*] \mathbf{H}_{\mathbf{X}}^\top \text{var}[\mathbf{Z}]^{-1} (\mathbf{Z}_{\mathbf{X}} - \mathbf{H}_{\mathbf{X}} \bar{\mathbf{X}} - \mathbb{E}[\mathbf{W}_{\mathbf{X}}]), \text{ and} \quad (21)$$

$$\text{var}_{\bar{\mathbf{X}}, \mathbf{Z}_{\mathbf{X}}}[\mathbf{X}^*] = \mathbf{J}_{n \times n} \otimes (\text{var}_{\bar{\mathbf{X}}}[\mathbf{X}_S^*] - \text{var}_{\bar{\mathbf{X}}}[\mathbf{X}_S^*] (\mathbf{H}_{\mathbf{X}}^S)^\top \text{var}[\mathbf{Z}]^{-1} \mathbf{H}_{\mathbf{X}}^S \text{var}_{\bar{\mathbf{X}}}[\mathbf{X}_S^*]), \quad (22)$$

where $\text{var}[\mathbf{Z}] = \mathbf{H}_{\mathbf{X}} \text{var}_{\bar{\mathbf{X}}}[\mathbf{X}^*] \mathbf{H}_{\mathbf{X}}^\top + \text{var}[\mathbf{W}_{\mathbf{X}}]$. These updates are shown in Figure 2c (for $\mathbb{E}_{\bar{\mathbf{X}}, \mathbf{Z}_{\mathbf{X}}}[\mathbf{X}^*]$) and Figure 2d (for marginal variance of $\text{var}_{\bar{\mathbf{X}}, \mathbf{Z}_{\mathbf{X}}}[\mathbf{X}^*]$), also for January. Figure 2e plots the contribution of the second update to our expected beliefs, $\mathbb{E}_{\bar{\mathbf{X}}, \mathbf{Z}}[\mathbf{X}^*] -$

$\mathbb{E}_{\bar{\mathbf{X}}}[\mathbf{X}^*]$. Regions of cooling are apparent westward of large continental masses (i.e. on the North American Pacific Coast, or the African Atlantic Coast). This is indicative of models not capturing up-welling phenomena, and is a pattern previously observed in the error between models and pre-industrial simulations (Eyring et al., 2019), as well as the cooling in the Southern Ocean, and warming the Indian and Pacific oceans. Larger uncertainty is seen in the Pacific where measurements are sparse.

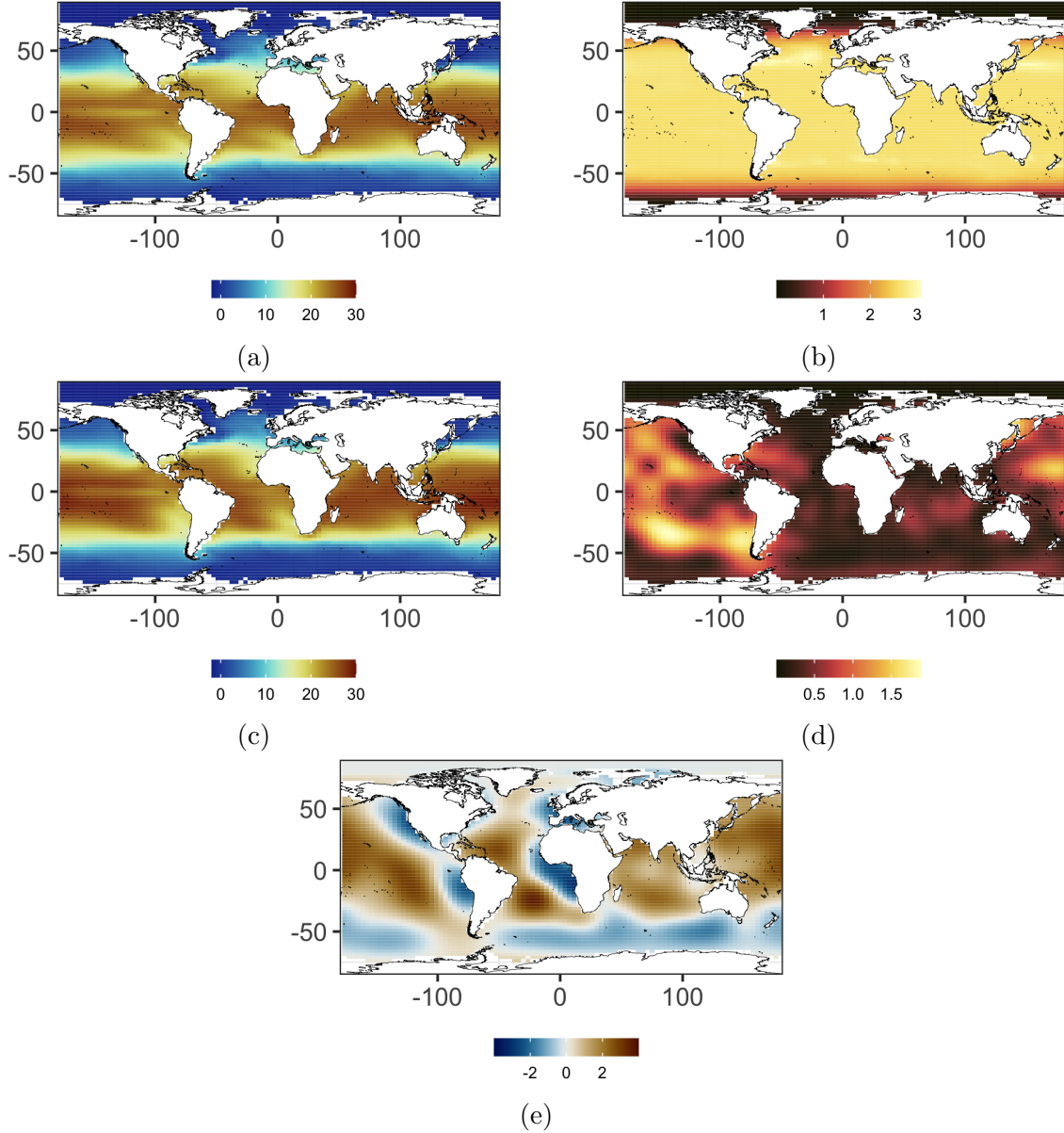


Figure 2: Adjusted beliefs of January SST: (a) adjusted expectation of SST by $\bar{\mathbf{X}}$, $\mathbb{E}_{\bar{\mathbf{X}}}[\mathbf{X}^*]$; (b) the adjusted variance of SST by $\bar{\mathbf{X}}$, $\text{var}_{\bar{\mathbf{X}}}[\mathbf{X}^*]$; (c) adjusted expectation of SST by $\bar{\mathbf{X}}$ and $\mathbf{Z}_{\mathbf{X}}$, $\mathbb{E}_{\bar{\mathbf{X}}, \mathbf{Z}_{\mathbf{X}}}[\mathbf{X}^*]$; (d) the adjusted variance of SST by $\bar{\mathbf{X}}$ and $\mathbf{Z}_{\mathbf{X}}$, $\text{var}_{\bar{\mathbf{X}}, \mathbf{Z}_{\mathbf{X}}}[\mathbf{X}^*]$; and (e) the contribution of the second update to our expected beliefs of SST $\mathbb{E}_{\bar{\mathbf{X}}, \mathbf{Z}_{\mathbf{X}}}[\mathbf{X}^*] - \mathbb{E}_{\bar{\mathbf{X}}}[\mathbf{X}^*]$. Temperature is shown in degrees Celsius and plots of variance show marginal variance.

4.2.2 Sea-ice concentration given sea-surface temperature

Following notation in Section 3 we now consider the process of SIC given SST. Define the jointly-observed ensemble of SST and SIC as $(\mathbb{X}, \mathbb{Y}) = \{(\mathbf{X}_1, \mathbf{Y}_1), \dots, (\mathbf{X}_m, \mathbf{Y}_m)\}$ where each \mathbf{Y}_i is a $12p$ -dimensional vector of SIC that we explicitly model as a function of SST, $\mathbf{Y}_i(\mathbf{X}_i)$. The $\mathbf{Y}_i(\mathbf{X}_i)$ comprise of 12 p -dimensional conditionally second order exchangeable spatial processes, $Y_{i,j}(X_{i,j})$, where i indexes the ensemble member and j indexes time. We assume $\mathbb{E}[Y_{i,j}(X_{i,j})] = \phi(X_{i,j})\beta_i$ which leads to the representation in (8), for which we require specifications of $\phi(X_{i,j})$, $\mathbb{E}[\beta_i]$, $\text{var}[\beta_i]$, and $\text{var}[\mathcal{R}_i(Y_i; X_i)]$. We assume the β_i to be second order exchangeable which leads to the representation in (9) that requires specification of $\mathbb{E}[\mathcal{M}(\beta)]$, $\text{var}[\mathcal{M}(\beta)]$ and $\text{var}[\mathcal{R}(\beta)]$. Together, these exchangeability judgements lead to the representation for the \mathbf{Y}_i in (10) (and equivalently (11)).

For modelling SIC given SST (and for most climate processes) we require spatial variation in the physics of the process. For example, the relationship between SIC and SST is different in the Nordic seas where sea-ice is supported at warmer SSTs than other locations. To account for this, we specify $\phi(X_{i,j}) = \Psi(X_{i,j})\Theta_i$ where $\Psi(X_{i,j})$ models the behaviour of SIC and SST at individual locations using spline bases, and Θ_i is a fixed-rank spatial basis of the spline coefficients. Note that we can model the spline coefficients individually in space, in which case $\phi(X_{i,j}) = \Psi(X_{i,j})$, but as the size of β_i then scales with the spatial resolution this is not feasible for climate models. Here we specify $\Psi(X_{i,j})$ with I-spline bases, a basis commonly used for monotone functions (such as SIC given SST). Θ_i is specified using a principal component design calculated using a projection of the \mathbf{Y}_i onto the column space of the $\Psi(\mathbf{X}_i)$, $\hat{\Theta}_i$. Approximating the spatial coefficients using principal components restricts inference for the β_i and $\mathcal{M}(\beta)$ to linear combinations of $\hat{\Theta}_i$; we argue this is appropriate for modelling the mean MME process. We use a more flexible parameterisation in the model discrepancy below so that inference on $\mathbf{Y}^*(\mathbf{X}^*)$ given the SIC data is not restricted to linear combinations of the principal component design. Full specification of $\Psi(X_{i,j})$ and the Θ_i is in the supplementary material. All $\Phi_i = \phi(\mathbf{X}_i)$ are full rank and so the conditions of Theorem 3.1 are met and $\hat{\beta} = (\hat{\beta}_1, \dots, \hat{\beta}_m)$ is sufficient for (\mathbb{X}, \mathbb{Y}) for updating $\mathbf{B} = (\beta_1, \dots, \beta_m, \mathcal{M}(\beta))$.

We specify $\text{var}[\mathcal{R}_i(Y_i; X_i)]$ as a heteroskedastic error process; smaller variance is specified for very cold SSTs (where we are confident there is sea-ice) and warm SSTs (where we are confident there is no sea-ice), and larger variance is specified for SSTs approximately between -1°C and 3°C where sea-ice behaviour is variable. Similar to Rougier et al. (2013) we set $\text{var}[\beta_i] = \lambda$ where λ is a diagonal matrix of the eigenvalues calculated from the principal component decomposition described above. As before we set $\text{var}[\mathcal{R}(\beta)] = \alpha^2 \text{var}[\mathcal{M}(\beta)]$.

Adjusted beliefs $\mathbb{E}_{\hat{\beta}}[\mathbf{B}]$ and $\text{var}_{\hat{\beta}}[\mathbf{B}]$ (and so to $\mathbb{E}_{\hat{\beta}}[\mathcal{M}(\beta)]$ and $\text{var}_{\hat{\beta}}[\mathcal{M}(\beta)]$) are calculated as in the supplementary material. As mentioned in Section 3.1 an advantage of specifying our model jointly over the β_i and $\mathcal{M}(\beta)$ is that we obtain inference for each β_i (as opposed to only $\mathcal{M}(\beta)$ as in Goldstein and Wooff (1998)). We look at the individual fits in Figure 3 where we plot SIC given SST, parameterised by the β_i , for each MME member, at four

locations. Location A shows a point in the Arctic where the models largely agree. Location B shows a region that occasionally sees small concentrations of sea-ice in the models but is predominantly too warm to support full sea-ice coverage. Location C shows three MME members whose relationship of SIC given SST disagrees with the rest of the ensemble (this is seen over the entire North Atlantic region and is not the result of a local erroneous fit). Finally, location D shows sea-ice behaviour at the Antarctic sea-ice edge. Given the SSTs that are observed, the differing physics predominantly lead to differences in Winter sea-ice.

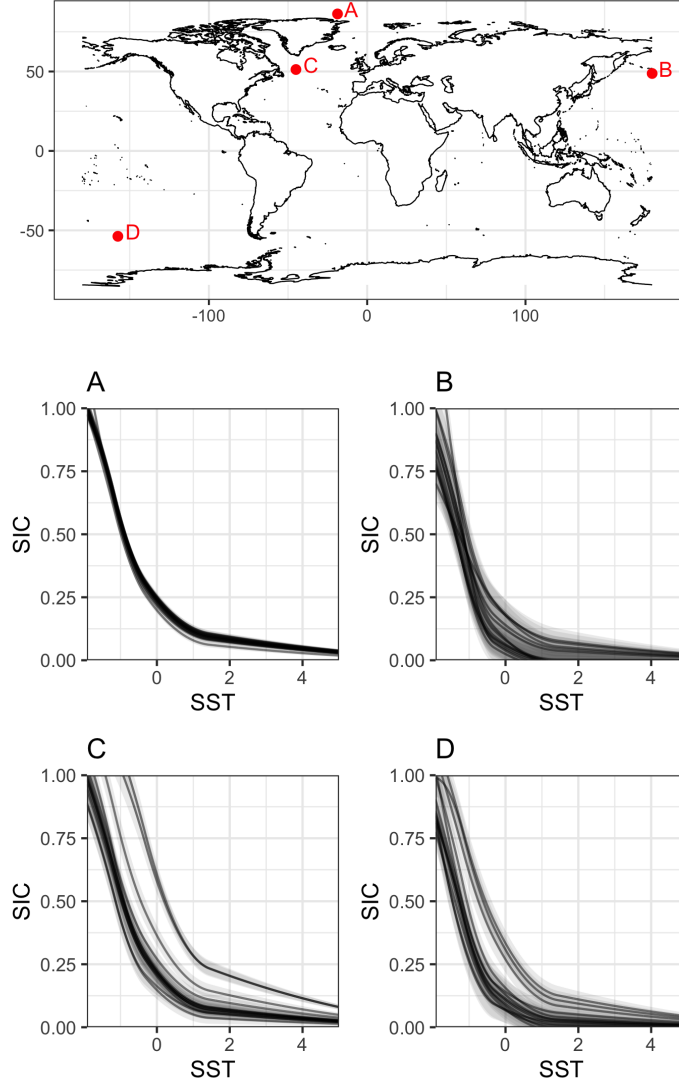


Figure 3: SIC given SST, parameterised by β_i , for each ensemble member, at four locations. Shaded regions denote ± 2 standard deviations.

Coexchangeability of $\mathbf{Y}^*(\mathbf{X}^*)$ and β_i leads to (13) for which specification of $A(\mathbf{X}^*)$, $\mathbb{E}[\mathbf{U}_{\mathbf{Y}}]$ and $\text{var}[\mathbf{U}_{\mathbf{Y}}]$ is required. We set $A(\mathbf{X}^*) = \phi(\mathbf{X}^*)$ and model discrepancy so that $\mathbf{U}_{\mathbf{Y}} = \Psi(\mathbf{X}^*)\mathbf{U}_{\Theta}$ (and thus $\mathbb{E}[\mathbf{U}_{\mathbf{Y}}] = \Psi(\mathbf{X}^*)\mathbb{E}[\mathbf{U}_{\Theta}]$ and $\text{var}[\mathbf{U}_{\mathbf{Y}}] = \Psi(\mathbf{X}^*)\text{var}[\mathbf{U}_{\Theta}]\Psi(\mathbf{X}^*)^{\top}$). \mathbf{U}_{Θ} represents the discrepancy of the spatial spline coefficients for the reality model. Should our MME contain models with high spatial resolution we could specify \mathbf{U}_{Θ} as a lower-rank

process (e.g. with fixed-rank methods such as Cressie and Johannesson (2008)); we do not find the need to do so here. We set $\mathbb{E}[\mathbf{U}_\beta] = 0$ and $\text{var}[\mathbf{U}_\Theta] = \mathbf{I}_{l \times l} \text{var}[\mathbf{U}_S]$ where l is the number of spline coefficients at each location and $\text{var}[\mathbf{U}_S]$ is calculated by the C^4 -Wendland function in (20) with parameters $\kappa^2 = 0.3$, $c = 4$, and $\tau = 6$. The first update $\mathbb{E}_{\hat{\beta}}[\mathbf{Y}^*(\mathbf{X}^*)]$ and $\text{var}_{\hat{\beta}}[\mathbf{Y}^*(\mathbf{X}^*)]$ is calculated given \mathbf{X}^* using $\mathbb{E}_{\hat{\beta}}[\mathcal{M}(\beta)]$ and $\text{var}_{\hat{\beta}}[\mathcal{M}(\beta)]$ as previously calculated. The second update $\mathbb{E}_{\hat{\beta}, \mathbf{Z}_Y}[\mathbf{Y}^*(\mathbf{X}^*)]$ and $\text{var}_{\hat{\beta}, \mathbf{Z}_Y}[\mathbf{Y}^*(\mathbf{X}^*)]$ are calculated given \mathbf{X}^* as in (17) and (18). Expectations and marginal variances of both updates, calculated with $\mathbf{X}^* = \mathbb{E}_{\bar{\mathbf{X}}, \mathbf{Z}_X}[\mathbf{X}^*]$ are shown in Figure 4. The expected SSTs do not produce adequate sea-ice when only considering learnt relations from the MME (Figure 4a) and marginal variance of SIC is large in regions where the expected SST is cold enough to support sea-ice (Figure 4b). Updating SIC using the data leads to more extensive sea-ice cover (Figure 4c) and a reduction of variance everywhere except the sea-ice boundary (Figure 4d). Similar behaviour is seen in the Northern Hemisphere winter.

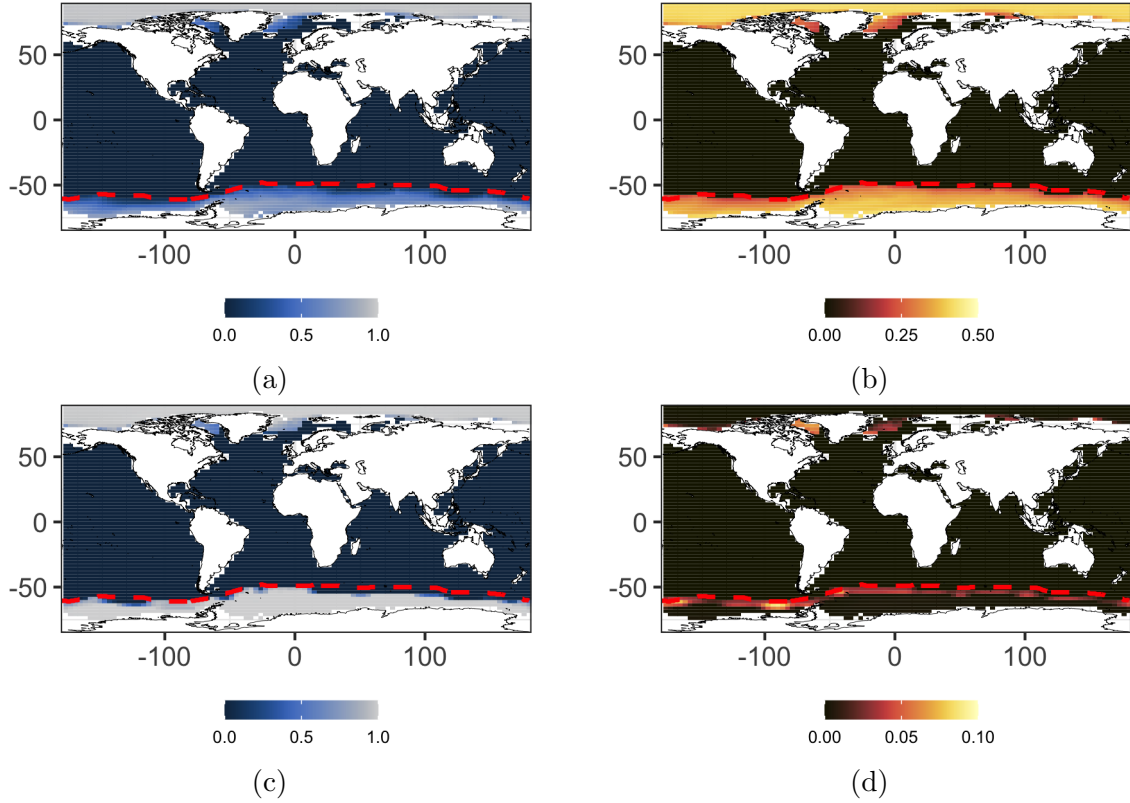


Figure 4: Adjusted beliefs of August SIC given expected SST (i.e. $\mathbf{X}^* = \mathbb{E}_{\bar{\mathbf{X}}, \mathbf{Z}_X}[\mathbf{X}^*]$): (a) the adjusted expectation of SIC by $\hat{\beta}$, $\mathbb{E}_{\hat{\beta}}[\mathbf{Y}^*(\mathbf{X}^*)]$; (b) the adjusted variance of SIC by $\hat{\beta}$, $\text{var}_{\hat{\beta}}[\mathbf{Y}^*(\mathbf{X}^*)]$; (c) the adjusted expectation of SIC by $\hat{\beta}$ and \mathbf{Z}_Y , $\mathbb{E}_{\hat{\beta}, \mathbf{Z}_Y}[\mathbf{Y}^*(\mathbf{X}^*)]$; and (d) the adjusted variance of SIC by $\hat{\beta}$ and \mathbf{Z}_Y , $\text{var}_{\hat{\beta}, \mathbf{Z}_Y}[\mathbf{Y}^*(\mathbf{X}^*)]$. Values are of sea-ice concentration and plots of variance show marginal variance.

5 Sampled boundary conditions and their influence on glacial ice sheet modelling outputs

The remit of this work was to reconstruct, with uncertainty, joint SST and SIC fields to act as boundary conditions into FAMOUS-Ice an ‘atmosphere only’ global climate model coupled to a ice sheet model. To briefly examine the effects that the reconstruction has on the atmosphere-ice sheet model outputs we run a small ensemble varying only the SST and SIC boundary conditions. To generate a joint sample $(\tilde{\mathbf{X}}^*, \tilde{\mathbf{Y}}^*)$, we first sample $\tilde{\mathbf{X}}^*$ and then $\tilde{\mathbf{Y}}^*(\tilde{\mathbf{X}}^*)$. As we have only expectations and variances for these quantities, we appeal to Chebyshev’s inequality to define a plausible set for $\{\mathbf{X}^*, \mathbf{Y}^*(\mathbf{X}^*)\}$, and sample this set uniformly (similar to how ensemble design is considered in history matching (Salter et al., 2019)). We sample

$$\tilde{\mathbf{X}}^* \sim \mathbb{E}_{\tilde{\mathbf{X}}, \mathbf{Z}_{\mathbf{X}}}[\mathbf{X}^*] + (\text{var}_{\tilde{\mathbf{X}}, \mathbf{Z}_{\mathbf{X}}}[\mathbf{X}^*])^{1/2} \mathbf{Z} \quad (23)$$

$$\tilde{\mathbf{Y}}^*(\tilde{\mathbf{X}}^*) \sim \mathbb{E}_{\hat{\beta}, \mathbf{Z}_{\mathbf{Y}}}[\mathbf{Y}^*(\tilde{\mathbf{X}}^*)] + (\text{var}_{\hat{\beta}, \mathbf{Z}_{\mathbf{Y}}}[\mathbf{Y}^*(\tilde{\mathbf{X}}^*)])^{1/2} \mathbf{Z} \quad (24)$$

where $(A)^{1/2}$ is any square-root decomposition of matrix A and $\mathbf{Z} \sim \mathcal{U}(-3, 3)$. An example of a joint sample $(\tilde{\mathbf{Y}}^*, \tilde{\mathbf{X}}^*)$ for the months of February and August is given in Figure 5.

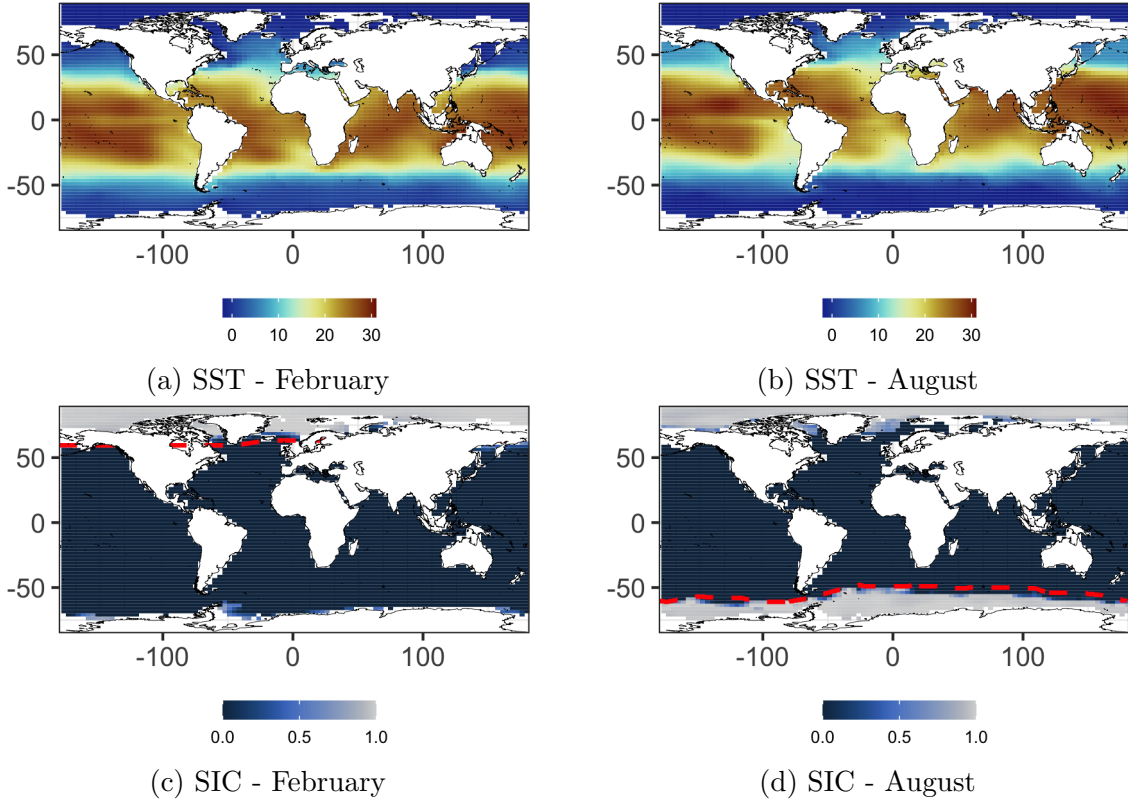


Figure 5: A single plausible sample from the SST and SIC reconstructions. Figures 5a and 5b show SSTs from February and August, respectively and Figures 5c and 5d show SICs from February and August, respectively.

We generate an ensemble of 25 runs comprising a single reference run utilising the

mean SST and SIC fields produced as part of the PMIP4 LGM experiments, and 24 randomly generated plausible samples of SST and SIC. Averaging over PMIP models to act as boundary conditions in ice-sheet modelling is commonplace (e.g. Kageyama et al. (2017)). Crucially, it should be noted that the reference run and each of the PMIP runs (\mathbb{X} , \mathbb{Y}) do not lie within the calculated plausibility bounds. To examine the impact of running with plausible boundary conditions, we compare reference and plausible ice sheet heights at four geographically distinct locations: Arctic Canada, Central Greenland, Hudson Bay, and the Pacific coast. This is shown in Figure 6. The simulator is run for 5000 years, with the ice sheet initialised with the LGM Glac-1D reconstruction (Tarasov et al., 2012). Beyond the SST and SIC fields, no other model parameters were changed and the model set-up was based on previous simulations of the Greenland ice sheet (Gregory et al., 2020).

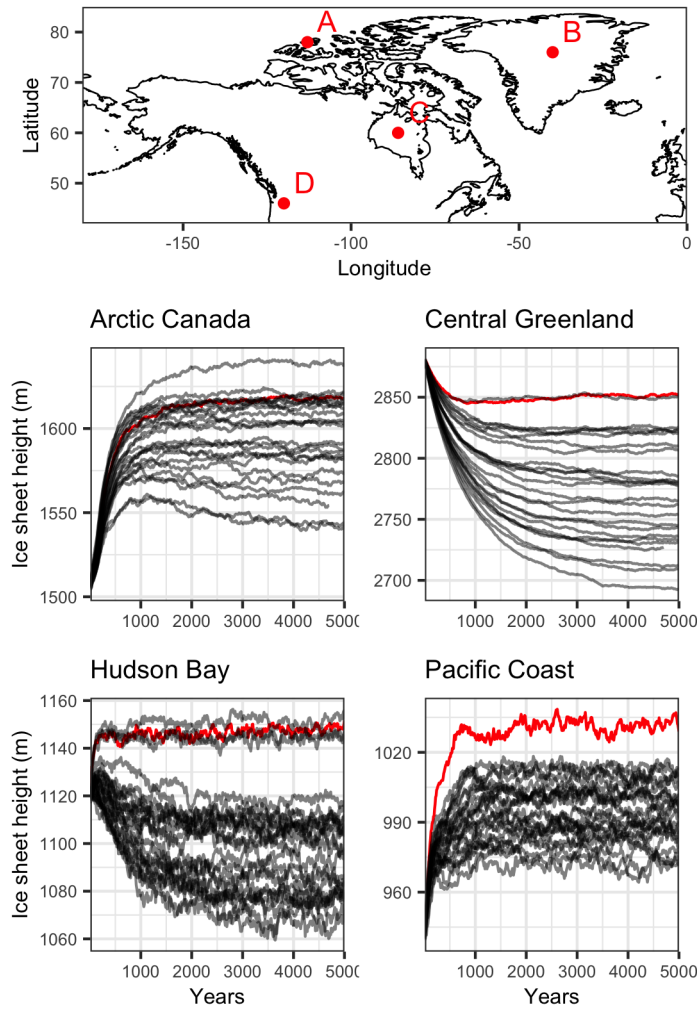


Figure 6: Ensemble time-series plots at four spatial locations: Arctic Canada (A), Central Greenland (B), Hudson Bay (C), and the Pacific Coast (D). The reference run is shown in red, the runs with varying SST and SIC fields in black.

Figure 6 shows that the boundary conditions have a strong influence on the simulated

ice sheet. SST and SIC can affect ice sheets either through changing the evaporation over the ocean that transforms into snow falling on the ice sheet, or by warming/cooling the regions close to the oceans thus affecting the surface melt rate. We find that the primary differences in ice sheet size are due to changes in snow accumulation. Our ensemble mainly produces lower ice elevation than the reference run. Examination of the individual ensemble members revealed that this was due to the cooler Eastern Pacific and Western Atlantic boundary conditions reducing evaporation over these oceans causing a reduction in the accumulation of snow onto the ice sheet.

The difference between the reference run and the samples is most pronounced at the Pacific coast. This matches our expectation that ocean-proximal sites are more sensitive to marine influence of the SST and SIC than more continental sites. This is also where we see the strongest reduction in SST in our samples compared to the PMIP4 model simulations. Indeed the second update causes a strong Pacific cooling along the coast of North America (Figure 2e) relative to the expectation based on the PMIP models. This is a region where models tend to underestimate the upwelling of cold waters from the deep ocean.

Such biases are common in climate models, but are particularly problematic for coupled climate-ice sheet models where the strong feedbacks between climate and ice sheets amplify the effects of climate biases, which can lead to runaway ice sheets (amplified growth or decay) and unrealistic geometries. The ensemble shows a substantial spread of ice elevation (5-10% of height) caused by the variance in reconstructed SST and SIC, highlighting the importance for considering this source of uncertainty for modelling past ice sheets. Our results show that correcting for biases and incorporating uncertainty in surface ocean conditions has a substantial effect on the simulated ice sheet, which in turn influences the internal dynamics of the ice sheet and its vulnerability to collapse or propensity to grow. The ice sheet geometry itself has direct impact on atmospheric circulation and an indirect influence on ocean circulation from runoff, thus directly impacting global heat distributions and surface climate conditions. Our methodology provides a way to reduce climate biases by prescribing ocean surface conditions compatible with observations, while at the same time exploring the effects of this source of uncertainty on other parts of the earth system.

6 Discussion

By exploiting natural conditional exchangeability judgements we develop theory for the coexchangeable process model, as an extension to Rougier et al. (2013), that combines multi-model ensembles and data to model correlated spatio-temporal processes. We provide results for efficient and scalable inference that may be used for large spatio-temporal problems where probabilistic Bayesian methods are often computationally infeasible (see, for example, Sansom et al. (2021)). Our methodology requires fewer assumptions and less onerous belief specifications than that required by a probabilistic Bayesian analysis.

To achieve these advancements we developed a Bayes linear analogue to a hierarchical Bayesian model. By combining exchangeability judgements and using the reparameterisation of Hodges (1998), we extend the Bayes linear exchangeable regressions methodology.

We obtain hitherto missing desirable properties present in traditional Bayesian hierarchical models such as shrinkage and the ability to make individual group level inference.

Large scale computational models often have complex spatio-temporal boundary conditions. This is particularly true for Earth system modelling, when any simulation of part of the Earth system, requires other spatio-temporal fields as boundary conditions. Our application looked at Palaeo ice-sheet modelling, where our model had a coupled atmosphere and ice-sheet, with the sea-surface temperature (SST) and sea-ice concentration (SIC) as prescribed boundary conditions. These are usually specified using results from a reference simulation, or using a member of a Model Intercomparison Project (MIP). However, individual simulations of Earth system components are known to have biases and any individual simulation cannot adequately represent uncertainty due to boundary conditions.

Our methodology allows MIP simulations to be combined with observations efficiently, leading to joint reconstructions of climate boundary conditions that can be used in any area of Earth System modelling. We demonstrated its efficacy by reconstructing last glacial maximum SST and SIC to force an ice-sheet model. We showed that the differences between reference ice-sheets and ice-sheets under plausible boundary conditions were considerable and that the uncertainty in the ice-sheet due to propagated boundary condition uncertainty was not ignorable.

Other aspects of the Earth system are likely to be sensitive to their boundary conditions, so that joint reconstructions of the type we present here would allow MIP simulations and data to be combined in order to correct existing biases and quantify an important source of uncertainty. The use of MIP ensembles to drive simulations of Earth system components leads to important questions around how these ensembles should be designed. Our method makes the case that a priori exchangeability across as many models as possible is an important design goal.

7 Acknowledgements

All authors were funded by UKRI Future Leaders Fellowship MR/S016961/1. Climate-ice sheet simulations were undertaken on ARC4, part of the High Performance Computing Facilities at the University of Leeds.

References

- Annan, J., Hargreaves, J.C., 2013. A new global reconstruction of temperature changes at the Last Glacial Maximum. *Climate of the Past* 9, 367–376.
- Astfalck, L., Cripps, E., Gosling, J., Milne, I., 2019. Emulation of vessel motion simulators for computationally efficient uncertainty quantification. *Ocean Engineering* 172, 726–736.
- Barthelmé, S., Chopin, N., 2014. Expectation propagation for likelihood-free inference. *Journal of the American Statistical Association* 109, 315–333.

- Benz, V., Esper, O., Gersonde, R., Lamy, F., Tiedemann, R., 2016. Last Glacial Maximum sea surface temperature and sea-ice extent in the Pacific sector of the Southern Ocean. *Quaternary Science Reviews* 146, 216–237.
- Bissiri, P.G., Holmes, C.C., Walker, S.G., 2016. A general framework for updating belief distributions. *Journal of the Royal Statistical Society. Series B, Statistical methodology* 78, 1103.
- Chandler, R.E., 2013. Exploiting strength, discounting weakness: combining information from multiple climate simulators. *Philosophical Transactions of the Royal Society A: Mathematical, Physical and Engineering Sciences* 371, 20120388.
- CLIMAP Project, 1981. Seasonal reconstructions of the Earth’s surface at the last glacial maximum. Geological Society of America.
- Cressie, N., Johannesson, G., 2008. Fixed rank kriging for very large spatial data sets. *Journal of the Royal Statistical Society: Series B (Statistical Methodology)* 70, 209–226.
- Crosta, X., Pichon, J.J., Burckle, L., 1998. Application of modern analog technique to marine Antarctic diatoms: Reconstruction of maximum sea-ice extent at the last glacial maximum. *Paleoceanography* 13, 284–297.
- De Finetti, B., 1975. *Theory of probability: A critical introductory treatment.* volume 1. John Wiley & Sons.
- De Vernal, A., Eynaud, F., Henry, M., Hillaire-Marcel, C., Londeix, L., Mangin, S., Matthießen, J., Marret, F., Radi, T., Rochon, A., et al., 2005. Reconstruction of sea-surface conditions at middle to high latitudes of the Northern Hemisphere during the Last Glacial Maximum (LGM) based on dinoflagellate cyst assemblages. *Quaternary Science Reviews* 24, 897–924.
- Eyring, V., Cox, P.M., Flato, G.M., Gleckler, P.J., Abramowitz, G., Caldwell, P., Collins, W.D., Gier, B.K., Hall, A.D., Hoffman, F.M., et al., 2019. Taking climate model evaluation to the next level. *Nature Climate Change* 9, 102–110.
- Gersonde, R., Crosta, X., Abelmann, A., Armand, L., 2005. Sea-surface temperature and sea ice distribution of the Southern Ocean at the EPILOG Last Glacial Maximum—a circum-Antarctic view based on siliceous microfossil records. *Quaternary Science Reviews* 24, 869–896.
- Goldstein, M., 1986. Exchangeable belief structures. *Journal of the American Statistical Association* 81, 971–976.
- Goldstein, M., Wooff, D., 2007. *Bayes linear statistics: Theory and methods.* volume 716. John Wiley & Sons.
- Goldstein, M., Wooff, D.A., 1998. Adjusting exchangeable beliefs. *Biometrika* 85, 39–54.

- Gregoire, L.J., Otto-Bliesner, B., Valdes, P.J., Ivanovic, R., 2016. Abrupt Bølling warming and ice saddle collapse contributions to the Meltwater Pulse 1a rapid sea level rise. *Geophysical research letters* 43, 9130–9137.
- Gregoire, L.J., Payne, A.J., Valdes, P.J., 2012. Deglacial rapid sea level rises caused by ice-sheet saddle collapses. *Nature* 487, 219.
- Gregory, J.M., George, S.E., Smith, R.S., 2020. Large and irreversible future decline of the greenland ice sheet. *The Cryosphere* 14, 4299–4322.
- Harrison, S.P., Bartlein, P., Izumi, K., Li, G., Annan, J., Hargreaves, J., Braconnot, P., Kageyama, M., 2015. Evaluation of CMIP5 palaeo-simulations to improve climate projections. *Nature Climate Change* 5, 735–743.
- Hodges, J.S., 1998. Some algebra and geometry for hierarchical models, applied to diagnostics. *Journal of the Royal Statistical Society: Series B (Statistical Methodology)* 60, 497–536.
- Hoff, P.D., 2009. A first course in Bayesian statistical methods. volume 580. Springer.
- Ivanovic, R., Gregoire, L., Kageyama, M., Roche, D., Valdes, P., Burke, A., Drummond, R., Peltier, W.R., Tarasov, L., 2016. Transient climate simulations of the deglaciation 21-thousand years before present; PMIP4 core experiment design and boundary conditions. *Geoscientific Model Development* 9, 2563–2587.
- Jesus, J., Chandler, R.E., 2011. Estimating functions and the generalized method of moments. *Interface focus* 1, 871–885.
- Kageyama, M., Albani, S., Braconnot, P., Harrison, S.P., Hopcroft, P.O., Ivanovic, R.F., Lambert, F., Marti, O., Peltier, W.R., Peterschmitt, J.Y., et al., 2017. The PMIP4 contribution to CMIP6–Part 4: Scientific objectives and experimental design of the PMIP4-CMIP6 Last Glacial Maximum experiments and PMIP4 sensitivity experiments. *Geoscientific Model Development* 10, 4035–4055.
- Kageyama, M., Harrison, S.P., Kapsch, M.L., Lofverstrom, M., Lora, J.M., Mikolajewicz, U., Sherriff-Tadano, S., Vadsaria, T., Abe-Ouchi, A., Bouttes, N., et al., 2021. The PMIP4 Last Glacial Maximum experiments: preliminary results and comparison with the PMIP3 simulations. *Climate of the Past* 17, 1065–1089.
- Kucera, M., Rosell-Melé, A., Schneider, R., Waelbroeck, C., Weinelt, M., 2005. Multiproxy approach for the reconstruction of the glacial ocean surface (MARGO). *Quaternary Science Reviews* 24, 813–819.
- Liu, X., Guillas, S., 2017. Dimension reduction for Gaussian process emulation: an application to the influence of bathymetry on tsunami heights. *SIAM/ASA Journal on Uncertainty Quantification* 5, 787–812.

- Masson, D., Knutti, R., 2011. Climate model genealogy. *Geophysical Research Letters* 38.
- Paul, A., Mulitza, S., Stein, R., Werner, M., 2020. A global climatology of the ocean surface during the Last Glacial Maximum mapped on a regular grid (GLOMAP). *Climate of the Past Discussions* , 1–26.
- Rougier, J., Goldstein, M., House, L., 2013. Second-order exchangeability analysis for multimodel ensembles. *Journal of the American Statistical Association* 108, 852–863.
- Salter, J.M., Williamson, D.B., Gregoire, L.J., Edwards, T.L., 2018. Quantifying spatio-temporal boundary condition uncertainty for the North American deglaciation. *arXiv preprint arXiv:1808.09322* .
- Salter, J.M., Williamson, D.B., Scinocca, J., Kharin, V., 2019. Uncertainty quantification for computer models with spatial output using calibration-optimal bases. *Journal of the American Statistical Association* 114, 1800–1814.
- Sansom, P.G., Stephenson, D.B., Bracegirdle, T.J., 2021. On constraining projections of future climate using observations and simulations from multiple climate models. *Journal of the American Statistical Association* , 1–12.
- Sarnthein, M., Gersonde, R., Niebler, S., Pflaumann, U., Spielhagen, R., Thiede, J., Wefer, G., Weinelt, M., 2003. Overview of glacial Atlantic Ocean mapping (GLAMAP 2000). *Paleoceanography* 18.
- Schmidt, G., Annan, J., Bartlein, P., Cook, B., Guilyardi, É., Hargreaves, J., Harrison, S., Kageyama, M., Legrande, A.N., Konecky, B., et al., 2014. Using palaeo-climate comparisons to constrain future projections in CMIP5. *Climate of the Past* 10, 221–250.
- Sha, Z., Rougier, J., Schumacher, M., Bamber, J., 2019. Bayesian model–data synthesis with an application to global glacio-isostatic adjustment. *Environmetrics* 30, e2530.
- Smith, R.S., George, S., Gregory, J.M., 2021. FAMOUS version xotzt (FAMOUS-ice): a general circulation model (GCM) capable of energy-and water-conserving coupling to an ice sheet model. *Geoscientific Model Development* 14, 5769–5787.
- Tarasov, L., Dyke, A.S., Neal, R.M., Peltier, W.R., 2012. A data-calibrated distribution of deglacial chronologies for the North American ice complex from glaciological modeling. *Earth and Planetary Science Letters* 315, 30–40.
- Tierney, J.E., Zhu, J., King, J., Malevich, S.B., Hakim, G.J., Poulsen, C.J., 2020. Glacial cooling and climate sensitivity revisited. *Nature* 584, 569–573.
- Whitaker, J.S., Hamill, T.M., 2002. Ensemble data assimilation without perturbed observations. *Monthly weather review* 130, 1913–1924.

- Williamson, D.B., Sansom, P.G., 2019. How are emergent constraints quantifying uncertainty and what do they leave behind? *Bulletin of the American Meteorological Society* 100, 2571 – 2588.
- Xiao, X., Fahl, K., Müller, J., Stein, R., 2015. Sea-ice distribution in the modern Arctic ocean: Biomarker records from trans-Arctic ocean surface sediments. *Geochimica et Cosmochimica Acta* 155, 16–29.
- Zhang, B., Cressie, N., et al., 2020. Bayesian inference of spatio-temporal changes of Arctic sea ice. *Bayesian Analysis* 15, 605–631.